First-Principles Modeling of Lithium Ordering in the LLTO ($Li_xLa_{2/3-x/3}TiO_3$) Superionic Conductor

Michele Catti*

Dipartimento di Scienza dei Materiali, Università di Milano Bicocca, via Cozzi 53, 20125 Milano, Italy

Received April 5, 2007. Revised Manuscript Received May 30, 2007

Ab initio periodic quantum-mechanical calculations were performed on selected ordered schemes of the La−Li−□ (vacancy) distribution in the $Li_{0.5}La_{0.5}TiO_3$ and $Li_{0.3125}La_{0.5625}□_{0.125}TiO_3$ phases. Perovskite superstructures were built on the basis of Z (formula units/primitive cell) = 4 and 8 in the first case (symmetries *C2me* to *Im*), and $Z = 16$ in the second one (*Pm*), with initial configurations from the experimental *P4*/*nbm* tetragonal structure of $Li_{0.3}La_{0.567}TiO_3$. The B3LYP functional (hybrid DFT/Hartree−Fock) was used, with an all-electron basis set of atomic orbitals (CRYSTAL06 code). For each ordered model, maps of the electrostatic potential were computed in the ionized unrelaxed superstructure, in order to study the field acting on Li^+ ions. The complete structure was then fully relaxed by energy minimization with respect to all atomic positions (78 atoms/cell in the $Z = 16$ case). The anti-phase octahedral tilt was reproduced for A-type cages with mixed La−Li composition in the same (001) layer, but not for full La−Li ordering in different layers. The optimized Li positions were found to lie in different sites within the A-cavities and depend significantly on the local environment. Experimental results of the average tetragonal LLTO structure could thus be explained, by finding correspondences between the observed Li sites and specific low-energy lithium ordered configurations.

1. Introduction

The lithium lanthanum titanates (LLTO) are among the phases exhibiting the highest ionic electrical conductivities at room temperature (about 1×10^{-3} S cm^{-1} for $x = 0.3$).[1,2] Their interest for applications in a variety of electrochemical devices has thus aroused intense research aimed at understanding the structural basis of this large Li^+ ion mobility. The LLTO chemical formula can be written as $Li_xLa_{2/3-x/3}□_{1/3-2x/3}TiO_3$, emphasizing the complex occupation pattern (including vacancies, □) of the A-type cage in the ABO_3 perovskite structure. Indeed, the goal of clarifying the subtle distortions of its basic perovskite arrangement and localizing lithium atoms within the large dodecahedral A-cavities has proved quite difficult, even by use of the choice technique of neutron diffraction.

We can summarize the main results in the literature by distinguishing between the Li-poor ($x < 0.24$) and Li-rich ($0.24 < x < 0.5$) phases. In the former case, a $2a_p \times 2a_p \times 2a_p$ superstructure with orthorhombic *Cmmm* space group was generally determined[3−8] (but for a quenched sample with $x = 0.18$, rhombohedral symmetry was instead reported[4,9]). For Li-rich compositions, tetragonal structures were mostly reported[10−14] and were recently shown[11,12] to correspond to $\sqrt{2}a_p \times \sqrt{2}a_p \times 2a_p$ rather than $a_p \times a_p \times 2a_p$ (as from earlier studies[13,14]) unit cells. However, rhombohedral[15] and orthorhombic[16,17] symmetries were also proposed for phases in this compositional range, and the situation is made more complicated by the structural dependence on the sample thermal history.[12] Independently of symmetry and compositional features, two main distortions are observed, at least in unquenched LLTO samples at room temperature, with respect to the ideal perovskite structure (a_p cubic cell edge). First, a partial ordering of the La−Li−□ substitution in the A-cages is observed along the *z*-axis; this causes the *c* cell edge to double from a_p to $2a_p$, so that alternate (001) layers of La-rich and La-poor A-type sites arise. Second, the TiO_6 octahedra tilt in anti-phase sequence around at least one of the crystallographic axes, which is *z* for tetragonal struc-

* Corresponding author. E-mail: catti@mater.unimib.it.

(1) Inaguma, Y.; Chen, L.; Itoh, M.; Nakamura, T.; Uchida, T.; Ikuta, H.; Wakihara, M. *Solid State Commun.* **1993**, *86*, 689.
(2) Kawai, H.; Kuwano, J. *J. Electrochem. Soc.* **1994**, *141*, L78.
(3) Inaguma, Y.; Katsumata, T.; Itoh, M.; Morii, Y. *J. Solid State Chem.* **2002**, *166*, 67.
(4) Varez, A.; Inaguma, Y.; Fernández-Diaz, M. T.; Alonso, J. A.; Sanz, J. *Chem. Mater.* **2003**, *15*, 4637.
(5) Sanz, J.; Alonso, J. A.; Varez, A.; Fernández-Diaz, M. T. *J. Chem. Soc., Dalton Trans.* **2002**, 1406.
(6) Sanz, J.; Varez, A.; Alonso, J. A.; Fernández-Diaz, M. T. *J. Solid State Chem.* **2004**, *177*, 1157.
(7) Varez, A.; Fernández-Diaz, M. T.; Alonso, J. A.; Sanz, J. *Chem. Mater.* **2005**, *17*, 2404.
(8) Yashima, M.; Itoh, M.; Inaguma, Y.; Morii, Y. *J. Am. Chem. Soc.* **2005**, *127*, 3491.
(9) Rivera, A.; Sanz, J. *Phys. Rev. B* **2004**, *70*, 094301.
(10) Varez, A.; Garcia-Alvarado, F.; Morán, E.; Alario-Franco, M. A. *J. Solid State Chem.* **1995**, *118*, 78.
(11) Sommariva, M.; Catti, M. *Chem. Mater.* **2006**, *18*, 2411.
(12) Catti, M.; Sommariva, M.; Ibberson, R. M. *J. Mater. Chem.* **2007**, *17*, 1300.
(13) Fourquet, J. L.; Duroy, H.; Crosnier-Lopez, M. P. *J. Solid State Chem.* **1996**, *127*, 283.
(14) Ruiz, A. I.; López, M. L.; Veiga, M. L.; Pico, C. *J. Solid State Chem.* **1999**, *148*, 329.
(15) Alonso, J. A.; Sanz, J.; Santamaria, J.; León, C.; Varez, A.; Fernández-Diaz, M. T. *Angew. Chem., Int. Ed.* **2000**, *39*, 619.
(16) Garcia-Martin, S.; Alario-Franco, M. A.; Ehrenberg, H.; Rodriguez-Carvajal, J.; Amador, U. *J. Am. Chem. Soc.* **2004**, *126*, 3587.
(17) Inaguma, Y.; Katsumata, T.; Itoh, M.; Morii, Y.; Tsurui, T. *Solid State Ionics* **2006**, *177*, 3037.

10.1021/cm0709469 CCC: $37.00
Published on Web 07/17/2007

tures[11,12] ($a^0a^0c^-$ scheme, according to Glazer's notation[18]) and usually *y* for orthorhombic structures[8,17] ($a^0b^-c^0$ scheme). An enlargement of the unit cell in the (001) plane from $a_p \times a_p$ to $\sqrt{2}a_p \times \sqrt{2}a_p$ (tetragonal) or $2a_p \times 2a_p$ (orthorhombic) ensues.

As for the lithium location within the A-type cages, three disordered (fractionally occupied) sites are reported in the few state-of-the-art neutron diffraction studies of LLTO phases: S1, intermediate between the A-cavity center and the center of the O_4 (vertical) window separating adjacent A-cages in the same (001) plane; S2, displaced from the cavity center along the *z*-direction, i.e., toward the above- or below-lying O_4 (horizontal) window center; S3, the vertical window center itself. Lithium was refined in S1 in the *I*4/*mcm* and *P*4/*nbm* tetragonal structures of the $x = 0.30$ phase[11,12] and in the *Cmmm* structure of the $x = 0.16$ and $x = 0.35$ terms.[3,17] The S2 site was detected but not Rietveld-refined in the former cases,[11,12] and site S3 was reported in the structures of the $x = 0.16$, 0.18, and 0.35 terms.[4,8,17] On the basis of these results, some models of mobility paths of Li^+ ions were devised,[11,12] also with the help of simple bond-valence-sum evaluations.[17,19] A primarily two-dimensional mechanism of ion hopping within the (001) plane ensues, in which site S3 acts mainly as bottleneck between the adjacent S1 sites; sites S2 may provide the connection for transfer between neighboring planes. Such models were substantially confirmed by molecular dynamics calculations.[20,21]

However, although a sufficiently clear picture of the complex structural properties of LLTO phases begins presently to be outlined, this is limited to statistically averaged configurations, such as those compatible with diffraction experiments. Solid-state NMR investigations of the Li^+ ion dynamics in LLTO were indeed performed,[22] detecting the presence of ions of two kinds with slightly differing environments, but much more detailed information on a local scale would be needed to untangle the complex disorder of the La−Li−□ distribution in the A cages. For this goal to be achieved, theoretical simulations of ordered arrangements of the LLTO structure, by state-of-the-art first-principles calculations of total energy, may be of great help. This was demonstrated, for instance, by a study of lithium ion mobility in the other important ionic material, $Li_{0.5}CoO_2$.[23] The only ab initio simulation of LLTO we are aware of was related to a hypothetical $Li_{0.25}La_{0.75}TiO_3$ phase with +3.5 formal oxidation state of Ti and no vacancies in the A-cage;[24] the least-energy position of lithium was searched for, but the relaxation of all other atoms in the structure was neglected.

We present here an accurate theoretical investigation of La−Li−□ ordering in $Li_xLa_{2/3-x/3}□_{1/3-2x/3}TiO_3$ phases, with emphasis on the two Li-rich compositions $x = 0.5$ and 0.3125. Periodic quantum-mechanical methods, based on the hybrid DFT (density functional theory)/Hartree−Fock B3LYP Hamiltonian with an all-electron localized basis set of atomic orbitals, are employed.[25] Two computational tools were exploited: determination of maps of electrostatic potential inside the ionized structure stripped of lithium atoms, and full energy minimizations with respect to all atomic positions for appropriately devised ordered models of the La−Li−□ distributions. The main aims are (1) to compare theoretical predictions of least-energy structural features (including Li positions) with the results of Rietveld refinements from neutron diffraction data, and consequently (2) to assign the different Li sites appearing in the experimental average structure to specific locally ordered configurations. This should contribute to a deeper insight into the structural basis of the Li^+ ion-mobility processes in the solid state.

2. Computational Methods

All quantum-mechanical calculations were carried out by the computer code CRYSTAL06,[25] implementing a periodic LCAO (linear combination of atomic orbitals) approach in which the self-consistent-field equations for one-electron eigenvalues and crystalline orbitals can be solved by using the DFT (density- functional theory) or Hartree−Fock Hamiltonian, or even mixtures of them. In this case, the B3LYP hybrid functional was used, including the DFT-LYP nonlocal correlation[26] and a mixture of the DFT Becke's[27] with the Hartree−Fock exchange. An all-electron localized basis set of Gaussian-type functions was employed for the radial parts of the AO's, corresponding to the Scheme 9(s)763311-(sp)631(d)G for La,[28] 8(s)6411(sp)31(d)G for Ti,[29] 8(s)411(sp)G for O,[29] and 6(s)1(sp)G for Li.[29] A total of 40, 27, 13, and 5 atomic orbitals ensued for each of the La, Ti, O, and Li atoms, respectively. The exponents of the outer Gaussians were optimized by energy minimization of the simplest ordered model of $Li_{0.5}La_{0.5}TiO_3$, with the experimental structural parameters (cf. below). The reciprocal space was sampled according to a regular sublattice defined by four points in each direction of the Monkhorst grid. The five tolerances related to cutoff limits for series summation were set to 1×10^{-7}, 1×10^{-7}, 1×10^{-7}, 1×10^{-7}, and 1×10^{-14}. Convergence was also controlled by a threshold ($\Delta E = 1 \times 10^{-8}$ hartree per primitive unit cell) in the SCF cycles. To accelerate the SCF convergence, we used the technique of level shifter, enhancing the energy difference between highest occupied and lowest unoccupied states in the first cycles. Atomic coordinates were optimized by calculation of analytical gradients and subsequent conjugate gradients algorithm (OPTCOORD option).

The electrostatic potential maps were computed for models built by supercells of the *P*4/*nbm* experimental structure of $Li_{0.3}La_{0.567}TiO_3$, as far as the Ti and O atoms are concerned,[12] with no atomic relaxation. The number and distribution of La atoms was changed appropriately in each model, and all lithium atoms were removed, so as to obtain charged ionic systems. Compensation of the ensuing negative charge was achieved by an uniform background positive

(18) Glazer, A. M. *Acta Crystallogr., Sect. B* **1972**, *28*, 3384.
(19) Mazza, D.; Ronchetti, S.; Bohnké, O.; Duroy, H.; Fourquet, J. L. *Solid State Ionics* **2002**, *149*, 81.
(20) Katsumata, T.; Inaguma, Y.; Itoh, M.; Kawamura, K. *Chem. Mater.* **2002**, *14*, 3930.
(21) Maruyama, Y.; Ogawa, H.; Kamimura, M.; Kobayashi, M. *J. Phys. Soc. Jpn.* **2006**, *75*, 064602.
(22) Emery, J.; Bohnké, O.; Fourquet, J. L.; Buzaré, J. Y.; Florian, P.; Massiot, D. *J. Phys.: Condens. Matter* **2002**, *14*, 523.
(23) Catti, M. *Phys. Rev. B* **2000**, *61*, 1795.
(24) Ono, S.; Seki, Y.; Kashida, S.; Kobayashi, M. *Solid State Ionics* **2006**, *177*, 1145.
(25) Dovesi, R.; Saunders, V.R.; Roetti, C.; Orlando, R.; Zicovich-Wilson, C.; Pascale, F.; Civalleri, B.; Doll, K.; Harrison, N. M.; Bush, I. J.; D'Arco, Ph.; Llunell, M. *Crystal06: User's Manual*; University of Torino, Italy, 2006; http://www.crystal.unito.it (accessed Sept 2006).
(26) Lee, C.; Yang, W.; Parr, R. G. *Phys. Rev. B* **1988**, *37*, 785.
(27) Becke, A. D. *J. Chem. Phys.* **1993**, *98*, 5648.
(28) Towler, M.D. http://www.tcm.phy.cam.ac.uk/~mdt26/crystal.html (accessed Sept 2006).
(29) http://www.crystal.unito.it (accessed Sept 2006).

Table 1. Unit Cells Used in the Simulations and Energy Values Obtained for the Different Optimized Ordering Models

unit-cell size	cell edges (Å)			Z
	a	b	c	
$a_p \times a_p \times 2a_p$	3.8761	3.8761	7.7464	2
$\sqrt{2}a_p \times \sqrt{2}a_p \times 2a_p$	5.4816	5.4816	7.7464	4
$2a_p \times 2a_p \times 2a_p$	7.7522	7.7522	7.7464	8
$2a_p \times 2a_p \times 4a_p$	7.7522	7.7522	15.4928	16

formula unit − S.G.	layer sequence	primitive cell	atoms/cell	E (hartree/f.u.)
$Li_{0.5}La_{0.5}TiO_3$				
C2me (*Aem2*)↓	2La/2Li − model (i)	$\sqrt{2}a_p \times \sqrt{2}a_p \times 2\ a_p$	20	
P2mm (*Pmm2*)		$a_p \times a_p \times 2a_p$	10	−5191.0445
Pa↓		$\sqrt{2}a_p \times \sqrt{2}a_p \times 2a_p$	20	
$P2_1am$ ($Pmc2_1$)		$\sqrt{2}a_p \times \sqrt{2}a_p \times 2a_p$	20	−5191.0444
Cmme↓		$\sqrt{2}a_p \times \sqrt{2}a_p \times 2a_p$	20	
Pmmm		$a_p \times a_p \times 2a_p$	10	−5191.0429
Im (*Cm*)	(3La + 1Li)/(1La + 3Li) model (ii)	$2a_p \times 2a_p \times 2a_p$	40	−5191.0410
Pm	(2La + 2Li)/(2La + 2Li) model (iii)	$2a_p \times 2a_p \times 2a_p$	40	−5191.0383
$Li_{0.3125}La_{0.5625}TiO_3$				
Pm	(3La + 1Li)/(2La + 1Li + 1□)/(3La + 1Li)/(1La + 2Li + 1□)	$2a_p \times 2a_p \times 4a_p$	78	−5703.6089

charge distribution in the reference cell (CHARGED option of the CRYSTAL code). The electrostatic potential values were evaluated at a grid of points by partitioning the periodic electron charge density in shell components; the short- and long-range contributions are calculated exactly and evaluated through a multipolar expansion of the shell components, respectively.[30,31] Maps of the potential were then obtained in different sections.

3. Results and Discussion

Two different "samples" of $Li_xLa_{2/3-x/3}\square_{1/3-2x/3}TiO_3$ were considered, with $x = 1/2$ and $x = 5/16$ lithium content. They both belong to the class of Li-rich compositions described in the experimental literature (see Introduction). All starting ordered structural models were built according to supercells of the experimental *P*4/*nbm* structure of the $Li_{0.3}La_{0.567}TiO_3$ term,[12] with Z ranging from 4 to 16. Every model is described as a sequence of (001) layers of A-type sites normal to the conventional z-axis of cubic perovskite. Each layer contains a number of A-sites per two-dimensional unit cell, which equals Z divided by the number of layers per unit cell. Layer symbols are adopted according to the following convention: 3La + 1Li means a layer with 4 A-type sites/2D cell, of which three are occupied by lanthanum and one by lithium atoms. In the subsequent least-energy structural optimizations, the lattice geometry was kept fixed and all atomic fractional coordinates were relaxed within symmetry constraints corresponding to orthorhombic or monoclinic space groups. The unit cells used for different models are summarized in Table 1.

3.1. $Li_{0.5}La_{0.5}TiO_3$. Three different ordering schemes were considered for this composition: (i) $Z = 4$, unit cell $\sqrt{2}a_p \times \sqrt{2}a_p \times 2a_p$ (2 layers with 2 sites/cell each), layer sequence 2La/2Li; (ii) $Z = 8$, $2a_p \times 2a_p \times 2a_p$ (2 layers with 4 sites/cell each), layer sequence (3La + 1Li)/(1La + 3Li); (iii) $Z = 8$, $2a_p \times 2a_p \times 2a_p$ (2 layers with 4 sites/cell each), layer sequence (2La + 2Li)/(2La + 2Li). In all cases, the size of the primitive cell has been indicated, with reference to the cubic perovskite cell edge a_p; nonprimitive unit cells will be specifically pointed out in the following, when necessary. For each scheme, the La−Li occupation pattern of the A-type sites has to be specified for every layer. Model (i) represents full ordering of La and Li in separate layers, model (ii) accounts for partial ordering such as that observed experimentally in the *P*4/*nbm* structure,[12] and model (iii) is appropriate for simulating full disorder of La−Li distribution along the z-axis, corresponding to the quenched *I*4/*mcm* phase.[11]

3.1.1. Model (i). This model, based on the same unit cell of the *P*4/*nbm* structure, is formed by a sequence of alternate layers in which all A-type sites are occupied either by lanthanum or by lithium atoms only. The electrostatic potential was computed before structure relaxation by removing all lithium atoms from the corresponding (001) layer. In Figure 1a, contour lines are shown on the empty Li layer 2Li (2□), with the apical oxygen atoms of TiO_6 octahedra therein appearing. The sides of the square correspond to the [110] and [−110] directions, with length equal to $2a_p$, and the perimeter of the $\sqrt{2}a_p \times \sqrt{2}a_p \times 2a_p$ unit cell is outlined inside. The absolute potential minima (−0.339 a.u.) are located at the centers (asterisks) of the vertical O_4 windows separating empty A-cavities; they are broad and elongated [110]. On the other hand, maxima of the potential (−0.314 a.u.) can be observed at the cavity centers. A map of the (−110) vertical section is shown in Figure 1b, where the z fractional coordinate is referred to $c = 2a_p$. From that, the window centers prove to be potential minima in all directions, whereas the cavity centers are saddle points with respect to the z-axis.

From a strictly electrostatic point of view, the most stable site for lithium ions is thus the window center (site S3). Ion hopping through the cavity center ([110] pathway) has to overcome an electric potential barrier of 0.025 a.u.=0.68 V; the lowest barrier between neighboring windows is yet only 0.19 V for tangential [100] pathways through saddle points (Figure 1a). However, bare electrostatics do not take into account the exchange repulsion (Li^+ ions have two 1s electrons), which tends to move lithium away from oxygen atoms with respect to the position of minimum electrostatic energy. This explains why, by minimizing the total quantum-mechanical energy, Li atoms are pushed off the window

(30) Saunders, V. R.; Freyria-Fava, C.; Dovesi, R.; Salasco, L.; Roetti, C. *Mol. Phys.* **1992**, *77*, 629.
(31) Saunders, V. R.; Freyria-Fava, C.; Dovesi, R.; Roetti, C. *Comp. Phys. Commun.* **1993**, *84*, 156.

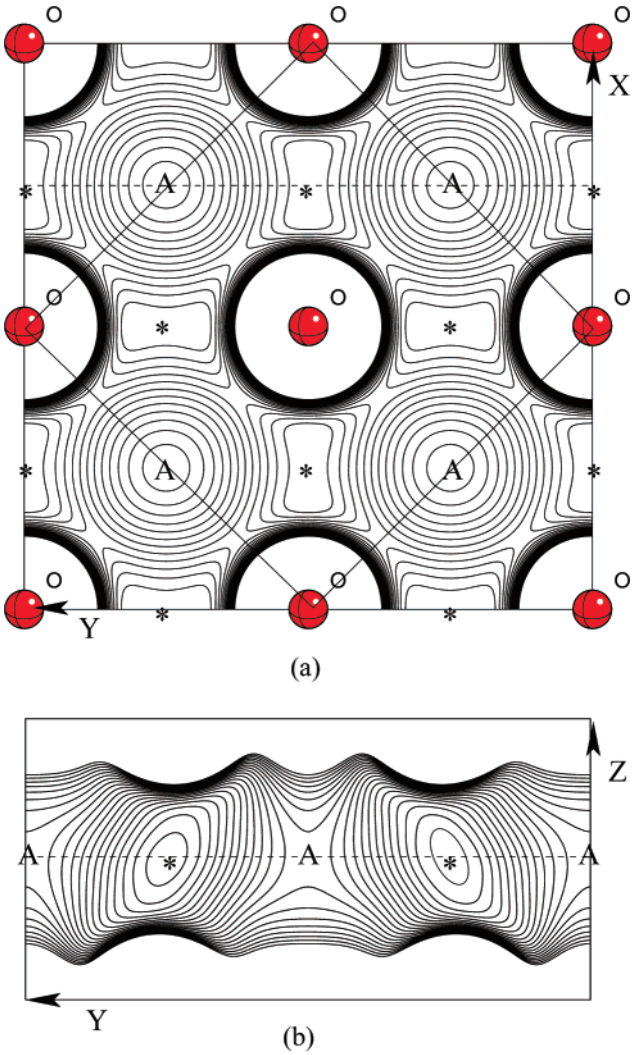

Figure 1. Maps of the electrostatic potential of $(La_{0.5}\square_{0.5}TiO_3)^{-0.5}$ with *P*4/*nbm* structure, referred to a $2a_p \times 2a_p \times 2a_p$ unit cell (the $\sqrt{2}a_p \times \sqrt{2}a_p \times 2a_p$ primitive cell is outlined in (a)); contour line separation of 0.002 a.u. (0.054 V). "A" letters and asterisks mark the centers of empty A-type cavities and of separating windows, respectively. (a) (001) layer at $z = 0$ with maxima (A) and minima (*). (b) Normal section through the dashed line of the previous figure. Saddle points (A) and minima (*) are shown.

centers (see below), consistent with most experimental evidence on Li-rich LLTO phases.

As in the lithium layer of model (i) there are two A-type cavities per unit cell, the initial structural configuration for relaxing the atomic coordinates is determined by arranging each of the two Li atoms in one of the four equivalent Li sites (S1) present in each cavity. Because of the minimum Li−Li distance requirement, there are only two possible configurations, sketched in Figure 2. The first one preserves the *m* plane, the second one the *a* (*b*) glide plane of the *P*4/*nbm* symmetry. The highest symmetries compatible with such arrangements are *C*2*me* (standard setting *Aem*2) and *Pa* (*Pc*) for case I and II, respectively. Structural optimizations were then carried out in both space groups, obtaining an unexpected result. In both cases, the final optimized structure had acquired an additional *m* plane normal to the *z*-axis, passing through the La layer and the Li layer and destroying the $a^0a^0c^-$ anti-phase octahedral rotation. In case I, the symmetry was increased to *P*2*mm* (*Pmm*2) with reduction of the unit cell to $a_p \times a_p \times 2a_p$ (symmetrical

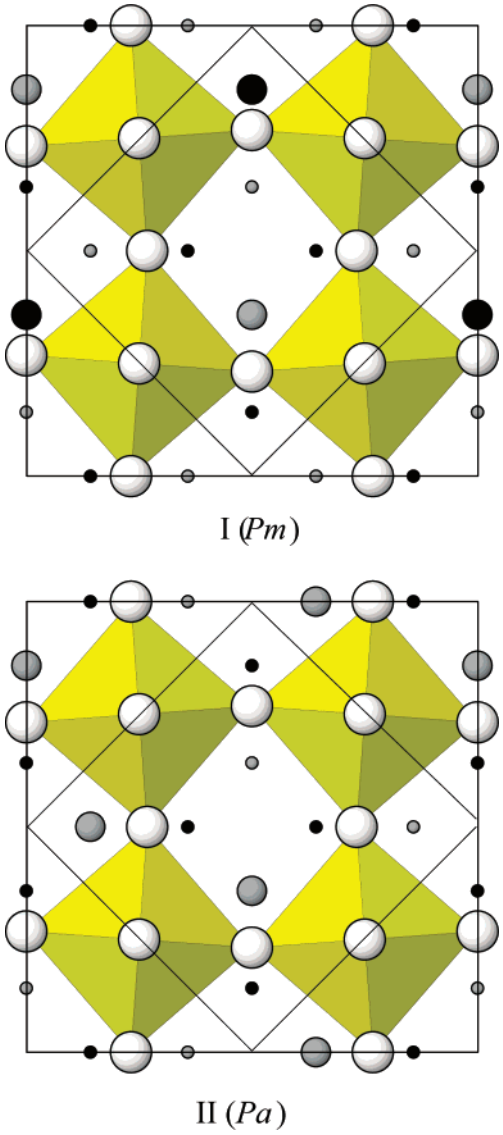

Figure 2. Ordered distributions of four Li atoms in perovskite A-type cavities, each containing four possible sites ($2a_p \times 2a_p$ layer cell, with the $\sqrt{2}a_p \times \sqrt{2}a_p$ cell outlined in thin lines). Tiny gray and black circles denote empty Li sites slightly above and below the plane of apical oxygen atoms, respectively. Intermediate gray and black spheres indicate Li atoms at corresponding levels. Actual atomic positions come from the experimental data of disordered *P*4/*nbm* $Li_{0.3}La_{0.567}TiO_3$.[12]

$a^0a^0c^0$ configuration), whereas in case II, the space group $P2_1am$ ($Pmc2_1$) was attained without change of the lattice periodicity, and the in-phase $a^0a^0c^+$ rotation appeared (Figure 3). This shows clearly that the full ordering of La and Li sites in separate homogeneous layers is not compatible with the anti-phase rotation observed experimentally. The reason will be clear after examining different ordered models based on mixed La−Li layers.

Although an important feature of the experimental structure such as the anti-phase tilt is not reproduced, these completely ordered models succeed in predicting the lithium atom positions correctly. In facts, Li is stabilized in approximately the same S1 site observed experimentally, i.e., off the center of the O_4 window separating adjacent A-type cavities in the same layer: see the fractional coordinates reported (Table 2) with reference to a larger $2a_p \times 2a_p \times 4a_p$ unit cell in order to make comparisons with other results easier. The coordinates of the other atoms in the optimized

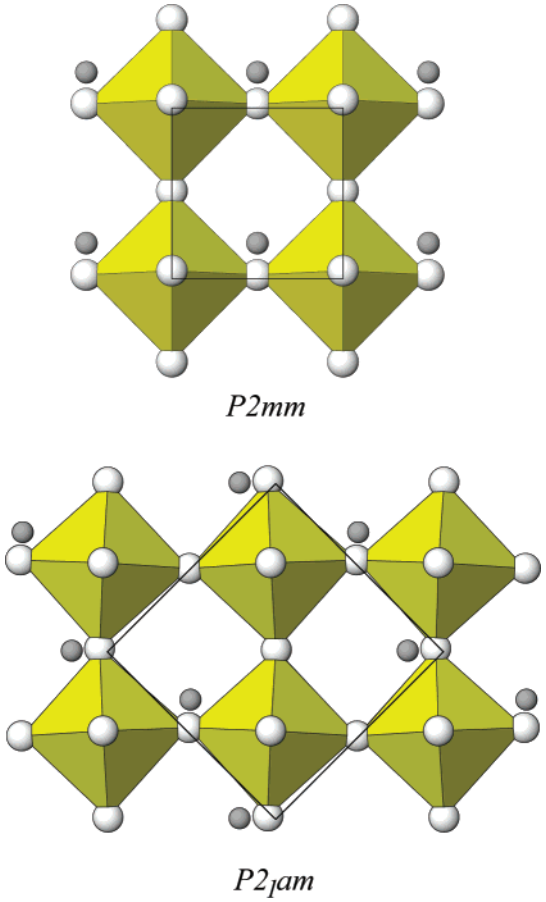

Figure 3. (001) layers, with Li atoms as gray spheres, in the optimized ordered structures of $Li_{0.5}La_{0.5}TiO_3$ according to *P2mm* and $P2_1am$ space groups. The $a_p \times a_p \times 2a_p$ (above) and $\sqrt{2}a_p \times \sqrt{2}a_p \times 2a_p$ (below) cells are outlined.

Table 2. Fractional Coordinates of Lithium Atoms in the Optimized Ordered Models of LLTO, and in the Experimental Disordered Structure of $Li_{0.3}La_{0.567}TiO_3$[12] (in all cases, reference is made to the largest unit cell ($2a_p \times 2a_p \times 4a_p$) for the sake of comparison, and the origin is referred to a La atom at $x = 0$, $y = 0$, $z = 0.125$)

		x	*y*	*z*
$Li_{0.3}La_{0.567}$ *P4/nbm* Exp.[12]	Li1	0.392	0	0.393
$Li_{0.5}La_{0.5}$ *P2mm*	Li1	0.3560	0	0.375
$Li_{0.5}La_{0.5}$ $P2_1am$	Li1	0.3595	0	0.375
$Li_{0.5}La_{0.5}$ *Im*	Li1	0.5091	0.5	0.1688
	Li2	0.0506	0.5	0.3406
	Li3	0.1684	0	0.3756
	Li4	0.6458	0	0.3740
$Li_{0.5}La_{0.5}$ *Pm*	Li1	0.3551	0.5	0.1177
	Li2	0.8554	0.5	0.1267
	Li3	0.1387	0	0.3772
	Li4	0.6388	0	0.3673
$Li_{0.3125}La_{0.5625}$ *Pm*	Li1	0.5122	0.5	0.1717
	Li2	0.3287	0	0.3718
	Li3	−0.0026	0	0.6802
	Li4	0.2004	0.5	0.8754
	Li5	0.7927	0.5	0.8752

structure are not given for brevity, but are available on request. A flattened pyramidal 4-fold coordination is shown by Li, with quite regular Li−O bond distances (Table 3).

The energy values obtained for versions I and II of the completely ordered model (i) are reported in Table 1. The difference of only 0.0001 hartree/f.u. is much smaller than the thermal energy at room temperature, and then hardly significant. To check the location of the lithium atom, we built and optimized a structure with Li lying exactly on the S3 site at the center of the O_4 window (space group *Cmme*) as well. Again, the symmetry increased to *Pmmm* with halving of the primitive cell, and the energy was 0.0016 hartree/f.u. (0.044 eV/f.u.) larger than the *P2mm* one (Table 1), thus confirming the off-center location of Li.

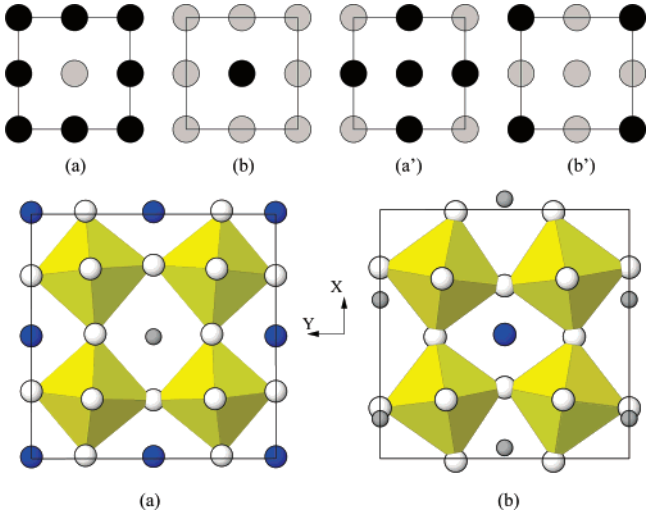

Figure 4. Above: Sequence of (3La + 1Li)/(1La + 3Li) (001) layers in the *Im* ordered model of $Li_{0.5}La_{0.5}TiO_3$ ($2a_p \times 2a_p \times 2a_p$ primitive and $2a_p \times 2a_p \times 4a_p$ conventional unit cells). Black and gray circles denote La- and Li-occupied A-type cavities, respectively; layers are superimposed from left to right. Below: Optimized configurations of the (a) 3La + 1Li and (b) 1La + 3Li independent layers; blue and white large spheres denote La and O atoms, and smaller gray spheres indicate Li atoms.

Some more complex ordered models ($Z = 8$, layer sequences 4La/4Li and 2La/2Li/2La/2Li′) were also devised, by doubling the size of the unit cell in order to accommodate lithium atoms in a greater number of independent positions within the A-type cavities (Figure 2). A superstructure *Pcmb* ($2a_p \times 2a_p \times 2a_p$) of the *C2me* model, and a superstructure $Pna2_1$ ($\sqrt{2}a_p \times \sqrt{2}a_p \times 4a_p$) of the *Pa* case were optimized. Again, the mirror plane normal to *z* appeared, increasing the symmetry to *Pcmm* and *Pnam*, respectively; further, the energy did not change appreciably. This confirms that the anti-phase tilting is prevented by the presence of pure La and Li layers and is not related to the ordering scheme of Li atoms within their cavities. Eventually, we also tested the effect of relaxing the unit-cell geometry together with the atomic coordinates: in the *P2mm* case, the values $a = 3.923$ Å, $b = 3.913$ Å, and $c = 7.921$ Å were obtained for the lattice constants, and −5191.0467 hartree for the energy. As expected from the behavior of the B3LYP functional, a slightly larger unit cell was optimized with respect to the experimental one, but the atomic coordinates did not change appreciably. Similar results were obtained for the $P2_1am$ structure as well, confirming the effects of unit-cell relaxation on the fractional coordinates to be negligible.

3.1.2. Model (ii). The second model considered is more realistic, insofar as it simulates a partial rather than full La−Li ordering along (001) layers. This is achieved by considering a two-layer primitive unit cell of double volume ($Z = 8$), with a (3La + 1Li)/(1La + 3Li) sequence. Two different mixed lanthanum−lithium layers are then included, with average occupation factors of La of 0.75 and 0.25, respectively (cf. 0.78 and 0.36 for experimental results of $Li_{0.3}La_{0.567}TiO_3$).[12] The patterns of La−Li occupation used are

Table 3. Average Ti−O and La−O Distances and rms Deviations (Å) in the Corresponding 6-Fold and 12-Fold Coordination Polyhedra, Respectively, for the Different Optimized Ordered Structures of LLTO (individual and average Li−O distances are also given)

	Ti−O		La−O		Li−O	<Li−O>
$Li_{0.3}La_{0.567}TiO_3$	1.945 0.022	La1	2.793 0.087	Li1	2.02, 2.43	2.18
P4/nbm Exp.[12]		La2	2.691 0.090		2.12 × 2	
$Li_{0.5}La_{0.5}$	1.949 0.076	La1	2.694 0.066	Li1	2.099 × 2	2.068
P2mm					2.036 × 2	
$Li_{0.5}La_{0.5}$	1.955 0.078	La1	2.698 0.145	Li1	1.999 × 2	2.033
$P2_1am$					1.988, 2.144	
$Li_{0.5}La_{0.5}$	1.963 0.098	La1	2.720 0.164	Li1	1.983, 2.098	2.267
Im					2.493 × 2	
	1.950 0.058	La2	2.697 0.184	Li2	2.073 × 2, 2.343	2.270
					2.431 × 2	
	1.955 0.058	La3	2.725 0.172	Li3	1.907, 2.035	2.053
					2.135 × 2	
	1.959 0.064	La4	2.724 0.146	Li4	2.048, 2.166	2.073
					2.039 × 2	
$Li_{0.5}La_{0.5}$	1.954 0.003	La1	2.713 0.177	Li1	1.989, 2.072	2.168
Pm					2.305 × 2	
	1.957 0.008	La2	2.713 0.177	Li2	1.988, 2.074	2.169
					2.307 × 2	
	1.957 0.008	La3	2.716 0.175	Li3	1.991, 2.080	2.175
					2.314 × 2	
	1.954 0.003	La4	2.716 0.175	Li4	1.990, 2.080	2.175
					2.315 × 2	
$Li_{0.3125}La_{0.5625}$		La1	2.684 0.156	Li1	1.975, 2.051	2.248
Pm					2.483 × 2	
		La2	2.724 0.169	Li2	1.924, 1.980	2.068
					2.183 × 2	
		La3	2.702 0.096	Li3	2.064, 2.128	2.102
					2.108 × 2	
		La4	2.700 0.162	Li4	1.885 × 2, 1.987	1.952
					2.050	
		La5	2.706 0.163	Li5	1.901, 1.917	1.938
					1.966 × 2	
		La6	2.679 0.106			
		La7	2.709 0.106			
		La8	2.712 0.147			
		La9	2.720 0.132			

shown in Figure 4 (above). By applying a centering repeat vector, and keeping just a mirror plane normal to layers, the *Im* symmetry arises (conventional unit cell $2a_p \times 2a_p \times 4a_p$, including four layers). The initial distribution of Li atoms over the available sites complied with the *m* symmetry (cf. Figure 2, I). Before optimization of the atomic coordinates, the lithium atoms were removed and maps of electrostatic potential were calculated. The results are not shown here for shortness, and they will be discussed below together with those related to the $Li_{0.3125}La_{0.5625}\square_{0.125}TiO_3$ composition.

After energy minimization, the structural arrangement shown in Figure 4 (below) was obtained. It appears immediately that in this case the anti-phase rotation of octahedra is reproduced correctly. The tilt angle is slightly larger in the 1La + 3Li than in the 3La + 1Li layer, but the alternate sequence of signs in subsequent layers corresponds to the $a^0a^0c^-$ scheme of the experimental average structure. As for the optimized Li positions, substantial changes are observed with respect to the initial configuration. In particular, in the 3La + 1Li layer, the single Li1 atom (Table 2) moves to a site located significantly above the center of the A-type cavity at 0.5, 0.5, and 0.125, far from the peripheral sites of the disordered experimental structure (Figure 2) and close to the experimental site S2. In the lithium-rich 1La + 3Li layer, Li2 goes again to a similar position as that of Li1 below the center of the cavity at 0, 0.5, and 0.375, whereas Li3 and Li4 keep close to their original experimental sites S1 (Table 2). On looking at the O-coordination of the four Li atoms (Table 3), it appears clearly that the latter two have quite regular 4-fold pyramidal environments, whereas Li1 and Li2 show a couple of long Li−O contacts (over 2.4 Å) and significantly larger average Li−O distances.

3.1.3. Model (iii). The scheme is again based on two La−Li independent layers with 4 A-type sites per layer, but in this case, they both have the same composition 2La + 2Li and are repeated by a perpendicular **c** vector rather than by a centering vector (**a** + **b** + **c**)/2, so as to give rise to a primitive *Pm* instead of centered *Im* monoclinic space group. Thus, a single *m* plane normal to layers is kept, out of the original symmetry operations, and Li atoms are constrained to lie on it. The average occupation factor of La is 0.5 in both layers, corresponding to the overall chemical composition. In Figure 5, the adopted pattern of La−Li distribution is shown. This rowlike pattern was chosen instead of a checklike pattern because it was more favorable for the process of lithium hopping involved in ionic mobility, as Li−Li distances are much shorter.

The optimized least-energy structures of both layers (Figure 5) show that, also in this case, the anti-phase octahedral tilt around *z* is simulated appropriately. A slight anti-phase rotation about the *x*-axis appears, too. All four Li atoms are located in positions close to the original experimental sites S1 (Table 2). However, their coordination environments are slightly more distorted than in the case of model (ii), because of the minor tilt around *x* that moves the apical octahedral O atoms slightly apart from the mirror planes where the Li atoms lie (Table 3).

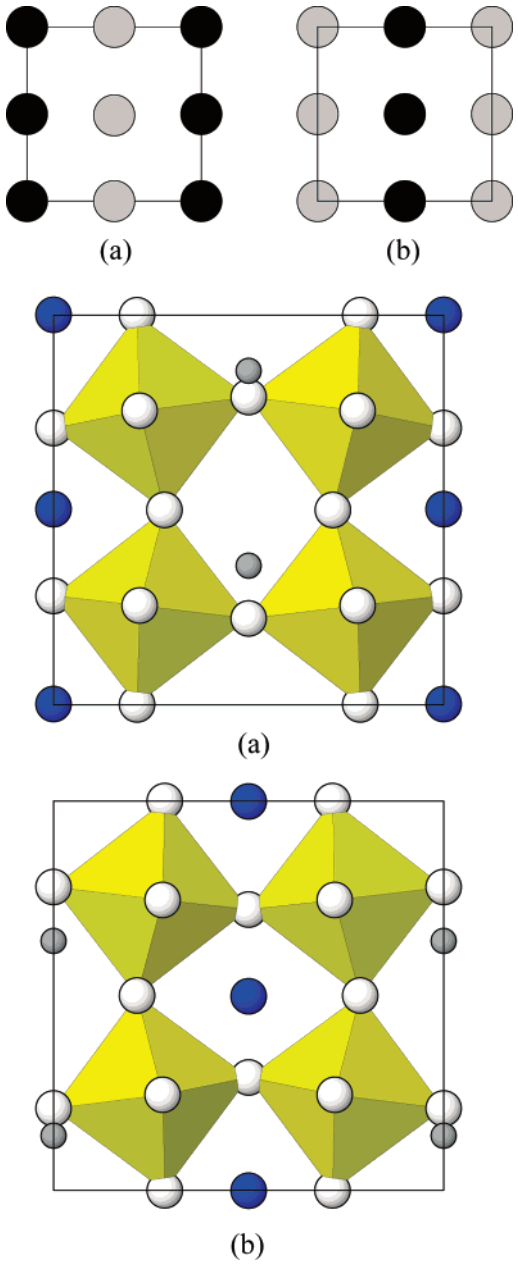

Figure 5. Above: Sequence of (2La + 2Li)/(2La + 2Li) (001) layers in the *Pm* ordered model of $Li_{0.5}La_{0.5}TiO_3$ ($2a_p \times 2a_p \times 2a_p$ unit cell). Black and gray circles denote La- and Li-occupied A-type cavities, respectively. Below: Corresponding optimized configurations of the two layers.

In summary, results from the three ordering models tested on $Li_{0.5}La_{0.5}TiO_3$ have proved that the mixed La−Li composition of (001) layers in the local atomic configurations is responsible for the anti-phase rotation of octahedra about the *z*-axis observed in the average experimental structure: indeed, this rotation is absent in model (i), where only pure (either La or Li) layers are present. Severe strains are produced by coexisting La and Li sites within the same layer (see the quite different La−O and Li−O bond lengths in Table 3), which are relieved by the $a^0a^0c^-$ octahedral tilt. The residual distortions of the 6- and 12-fold Ti and La coordination polyhedra can be appreciated by looking at the root-mean-square deviations of Ti−O and La−O bond lengths (Table 3), which show larger values for the La polyhedra in mixed layers like 3La + 1Li, 1La + 3Li, and 2La + 2Li (*Im* and *Pm* models).

As for the Li location, two different kinds of sites have been detected by energy minimization. One of them corresponds roughly to the one refined in the quoted experimental studies[11,12] of $Li_{0.3}La_{0.567}TiO_3$ (Li n.1), and denoted as S1 in the Introduction; it lies at about 0.6−0.9 Å along the *x*-axis from the center of the window separating adjacent A-type cavities within the layer, which in turn is located at $x = 0.25$ or 0.75, and $y = 0$ or 0.5 (see Figures 2, 4, and 5). All Li atoms but Li1 and Li2 of model *Im* (ii) (see Table 2) take this position. The latter lithium atoms, on the other hand, occupy a site located just vertically above or below the center of the A-type cavity, at $x = 0$ or 0.5 and $y = 0.5$, at a distance of 0.5−0.7 Å along *z*. This site resembles roughly the one that was reported as peak Li n.2 from the Fourier difference maps in both the *I*4/*mcm* and *P*4/*nbm* Rietveld-refined structures by neutron diffraction data of $Li_{0.3}La_{0.567}TiO_3$ (site S2 in the Introduction). That peak of neutron density was located at 1.19 Å (*P*4/*nbm*)[12] or 1.09 Å (*I*4/*mcm*)[11] from the center of the A-type cavity, vertically along *z*. Therefore, we are now able to relate the two different Li positions detected experimentally in the average structure to specifically distinct local configurations surrounding lithium atoms. In particular, when the Li cavity is surrounded by La atoms all around, then the S2 site should be occupied (see Li1 in the 3La + 1Li layer of the *Im* model).

A final consideration concerns the relative energies of models (i), (ii), and (iii) (Table 1). It appears clearly that the total energy increases with disorder, i.e., from pure layers of either La or Li (i), to mixed layers richer in either atom (ii), to mixed layers of La−Li balanced composition (iii). A given layer arrangement is then energetically destabilized as the number of coexisting La and Li cavities per unit volume grows, although of course its configurational entropy increases, so that the overall free-energy balance is expected to be ruled by temperature. A simple combinatorial calculation gives configurational entropies $S(\text{ii}) = R\ln 16$ and $S(\text{iii}) = R\ln 36$, so that the corresponding free energies are $\Delta F(\text{ii}-\text{i}) = 9190 - 23.05T$, and $\Delta F(\text{iii}-\text{i}) = 16279-29.80T$ J mol^{-1}. It is confirmed that model (iii) corresponds to a high-temperature state, model (ii) is adequate to represent an intermediate temperature structure, and model (i) is an ideal full-order configuration at 0 K (athermal limit).

3.2. $Li_{0.3125}La_{0.5625}\square_{0.125}TiO_3$. For compositions with $x < 0.5$, vacancies have to be introduced into the ordered configurations. The simplest model corresponding to the lithium content of $x \approx 1/3$ is based on 9 La, 5 Li, and 2 □ per $2a_p \times 2a_p \times 4a_p$ unit cell ($Z = 16$), corresponding to 4 layers with 4 sites/cell each. By the above constraints on the atomic contents of the unit cell, only the following 12 layer compositions are possible: 2La + 1Li + 1□ (12), 1La + 2Li + 1□ (12), 1La + 1Li + 2□ (12), 2La + 2Li (6), 2La + 2□ (6), 2Li + 2□ (6), 3La + 1Li (4), 3La + 1□ (4), 1La + 3Li (4), 3Li + 1□ (4), 4La (1), 4Li (1). The arrangements have been ordered according to decreasing multiplicity of layer configurations, indicated in parentheses; the layer multiplicity is equal to $4!/[n(\text{La})!n(\text{Li})!n(\square)!]$. Therefore, a great number of possible layer sequences complying with the given chemical composition arises. To select the sequence for our model, we have given priority to

two criterions: large total multiplicity of configurations (entropic criterion), and suitability for the study of lithium transfer processes. The total multiplicity is simply the product of multiplicities of the four selected layers. The second criterion would favor the La-poor layers with rowlike rather than checklike Li−Li or Li−□ neighboring cavities. The layer sequence (3La + 1Li)/(2La + 1Li + 1□)/(3La + 1Li)/(1La + 2Li + 1□), with a total multiplicity of 2304 configurations, complies with both criteria satisfactorily and was thus selected for the simulations. Similar layer configurations were adopted in the 3La + 1Li, 1La + 3Li, and 2La + 2Li cases of models (ii) and (iii) of the $Li_{0.5}La_{0.5}TiO_3$ composition (see Figures 4 and 5), regardless of substitutions of Li atoms by vacancies in the A-type cavities. Thus, the mirror plane constraint was kept, too, giving rise again to the monoclinic *Pm* symmetry. The ensuing model, based on 78 atoms per primitive unit cell (Table 1), presented the largest computational weight of this work.

At first, the lithium atoms were removed from the structure, keeping all other atomic positions fixed at their "experimental" values, and the electrostatic potential was evaluated on each of the four independent layers. Corresponding contour-line maps are shown for the 2La + 1Li + 1□ (now 2La + 2□) and 1La + 2Li + 1□ (now 1La + 3□) layers in Figures 6 and 7, respectively. The maps of Figure 6 are similar to those obtained previously for the equivalent 2La + 2Li (2La + 2□) layer of model (iii), and the maps of Figure 7 resemble those of the 1La + 3Li (1La + 3□) layer of model (ii) of the $Li_{0.5}La_{0.5}TiO_3$ sample, which for this reason have not been reported.

In the 2La + 1Li + 1□ (2La + 2□) case, the rowlike distribution of La atoms gives rise to parallel tunnels of vacancies in which the lithium ions can be transferred with one-dimensional hopping (Figure 6a). In the (001) plane, potential minima (−0.409 a.u.) and saddle points (−0.390 a.u.) are observed exactly at the window centers and at the cavity centers, respectively, with an electrostatic barrier of 0.52 V. The vertical section (Figure 6b) shows both the previous 2La + 2□ layer (below, crossed by a dashed line), and the upper one 3La + 1□ (above), where a more complex situation is noticed. First, the minima corresponding to window centers in Figure 6a are displaced upward (B, −0.412 a.u.); this could be expected, as it was already remarked that electrostatic potential minima tend to be closer to oxygen atoms than the actual Li positions, because exchange repulsion is not taken into account. Second, the empty cavity A sandwiched between two La sites in the vertical plane, and the A′ one neighboring another empty cavity (A″) in the next layer, behave differently. The central site A is a real saddle point in three dimensions, whereas the A′ center lies on a slope declining toward the area around the adjacent A″ cavity in the upper layer, where minima in C (−0.459 a.u.) and in D (−0.471 a.u.) are observed (Figure 6b). This shows that the A″ cavity, surrounded by La sites in the 3La + 1□ layer, may be a trapping hollow for lithium ions hopping throughout the crystal structure.

A two-dimensional network of empty tunnels is observed in the 1La + 3Li (1La + 3□) layer (Figure 7a). The A-cavities show exactly the same pattern of potential isolines,

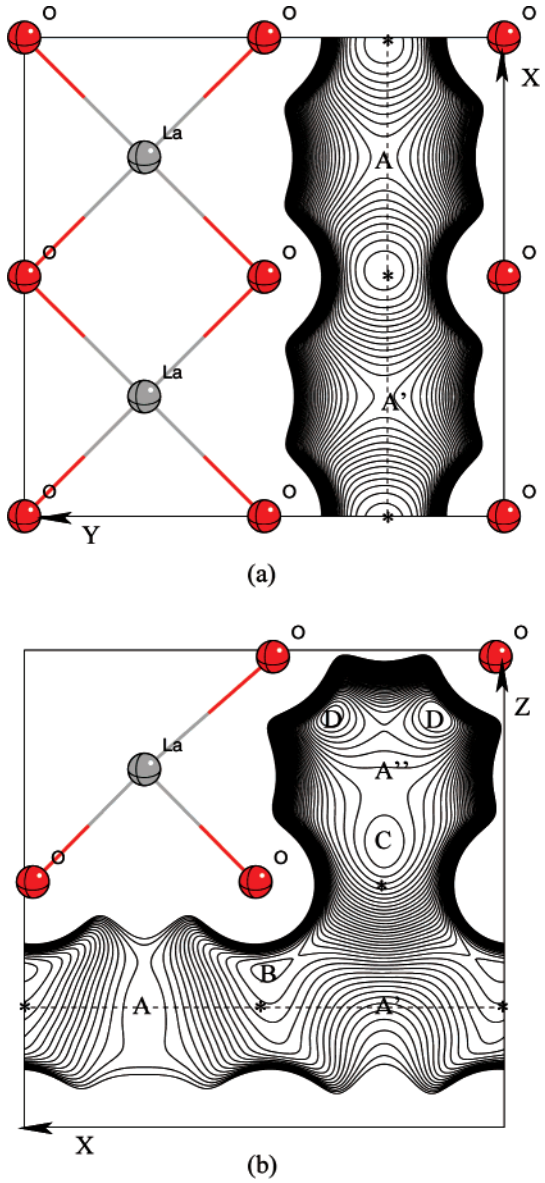

Figure 6. Maps of the electrostatic potential of $(La_{0.5625}\square_{0.4375}TiO_3)^{-0.3125}$ with *Pm* structure and $2a_p \times 2a_p \times 4a_p$ unit cell; contour line separation 0.002 a.u. (0.054 V). Window centers and empty A-type sites are marked by asterisks (*) and "A" letters, respectively. (a) (001) 2La + 2□ layer at $z = 0.375$ with minima (*) and saddle points (A, A′). (b) Normal section through the dashed line of (a); a saddle point (A) and three minima (B−D) are indicated.

also in the vertical plane (Figure 7b), as the corresponding ones in the previous layer (Figure 6): the central saddle point lies at −0.446 a.u. The A′ cavity, neighboring a A″ hollow in the above 3La + 1Li (3Li + 1□) layer (Figure 7b), is located at the crossings of perpendicular tunnels, and thus differs from the corresponding one of the previous case, where this topological feature was absent. In fact, instead of a saddle point, we observe on the (001) plane a broad area of low potential around the A′ center, which is itself a weak local maximum (−0.480 a.u.) surrounded by four minima (B) at −0.484 a.u. These are located very close to the experimental positions of Li in *P*4/*nbm* $Li_{0.3}La_{0.567}TiO_3$ (Li n.1).[12] When the vertical section is considered, however, then the absolute minimum is seen to drift toward the center of the window separating the A′ and A″ cavities (−0.518 a.u.). This resembles what is observed in the 2La + 1Li +

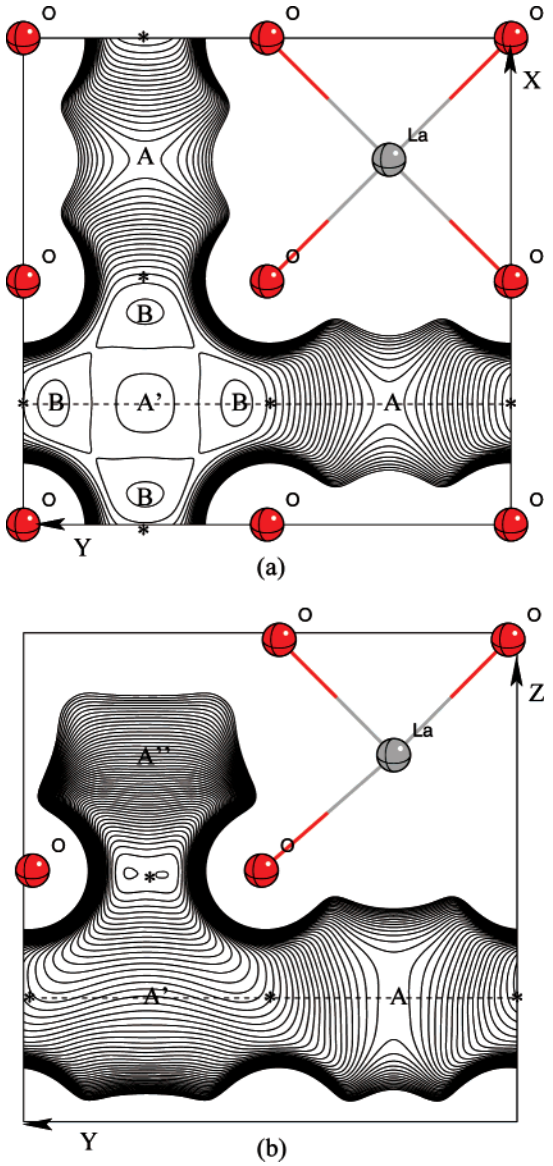

Figure 7. Maps of the electrostatic potential of $(La_{0.5625}\square_{0.4375}TiO_3)^{-0.3125}$ with *Pm* structure and $2a_p \times 2a_p \times 4a_p$ unit cell; contour line separation 0.002 a.u. (0.054 V). Window centers and empty A-type sites are marked by asterisks and "A" letters, respectively. (a) (001) 1La + 3□ layer at $z = 0.875$ with minima (B), saddle points (A), and maximum (A′). (b) Normal section through the dashed line of (a); a minimum (*) and a saddle point (A) appear.

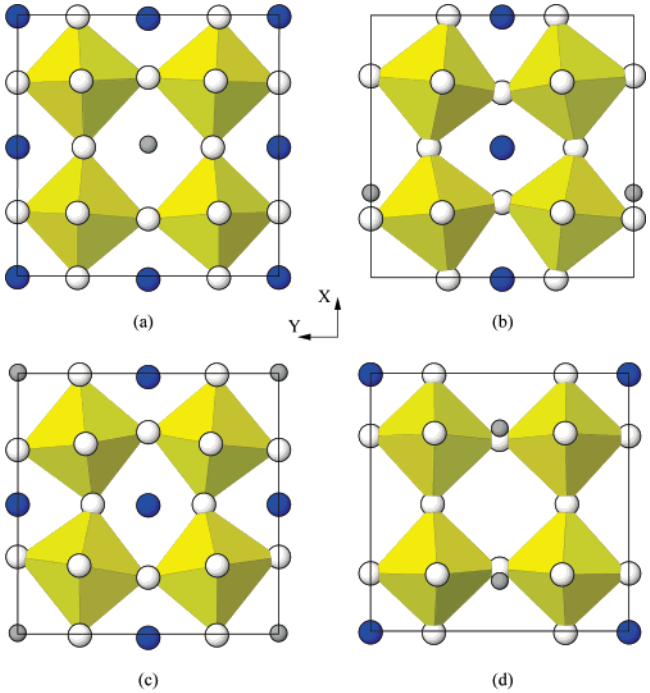

Figure 8. Least-energy optimized configurations of the (a) 3La + 1Li, (b) 2La + 1Li + 1□, (c) 3La + 1Li, and (d) 1La + 2Li + 1□ layers in the *Pm* ordered model of $Li_{0.3125}La_{0.5625}\square_{0.125}TiO_3$ ($2a_p \times 2a_p \times 4a_p$ unit cell). The *z* coordinate increases from (a) to (d).

1□ (2La + 2□) layer, although now the minima in D (Figure 6b) are no more present.

After including Li atoms and relaxing all atomic coordinates, we obtained the least-energy structure shown in Figure 8. By comparison with the corresponding results for previous models of the different $Li_{0.5}La_{0.5}TiO_3$ composition based on the $2a_p \times 2a_p \times 2a_p$ unit cell ($Z = 8$, see Figures 4 and 5), one can establish that the structure of a layer with a given arrangement of La atoms is substantially the same, independently of the Li−□ distribution in the other cavities and of the type of neighboring layers. This confirms the behavior already remarked for the electrostatic potential of equivalent layers in different compositional models. In particular, when the Li-occupied cavity is surrounded by La-occupied sites, the Li atom invariably goes to the (*x*,*y*) cavity center, but displaced somehow along *z* (panels a and c in Figure 8 and Figure 4a): see the coordinates of Li1 and Li3 of the present case and Li1 of $Li_{0.5}La_{0.5}$ *Im* (Table 2). This site corresponds roughly to that of the neutron density peak Li n.2 detected in the experimental studies of tetragonal $Li_{0.3}La_{0.567}TiO_3$ and denoted here as S2. A similar position is taken also by Li2 of $Li_{0.5}La_{0.5}$ *Im* (Figure 4b), which is confined by two neighboring La sites along the *x*-axis and blocked by the mirror plane on which it lies in the perpendicular *y* direction. On the other hand, when no La atoms are present along the *x*-axis, the Li atoms are then free to take their preferred position off the center of the O_4 window separating adjacent cavities (Table 2), which corresponds to Li n.1 of the experimental tetragonal structure (site S1). The distance from the window center can vary somehow, as shown by the $2a_p|x - 0.25|$ value for Li2 (1.22 Å) and Li4 (0.77 Å), and by $2a_p|x - 0.75|$ for Li5 (0.66 Å) (Table 2).

4. Conclusions

The locally ordered La−Li−□ configurations of the ion conducting phases $Li_{0.5}La_{0.5}TiO_3$ and $Li_{0.3125}La_{0.5625}\square_{0.125}TiO_3$ have been modeled successfully by accurate ab initio quantum-mechanical techniques. In particular, the anti-phase $a^0a^0c^-$ octahedral tilt, observed experimentally in $Li_{0.3}La_{0.567}TiO_3$, has been demonstrated to depend strictly on the mixed La−Li local composition of (001) layers.

By analyzing the electrostatic potential distribution in the Li-free ionized structure, we have obtained useful preliminary insight into the actual lithium location; this has then been determined reliably by subsequent extensive least-energy structural optimizations of several ordered models. Their results prove the location of Li inside a given A-type cavity to depend solely on the pattern of La−(Li,□) occupation of the first-neighboring cavities. In particular, four different

main configurations are outlined within a layer: (1) A-cage surrounded by four La atoms; (2) A-cage neighboring two La atoms along a row and two (Li,□) cavities along the perpendicular row; (3) A-cage surrounded by four (Li,□) cavities, with La atoms in check pattern; (4) A-cage in a layer of (Li,□) cavities only. A secondary role may be played also by the La−(Li,□) occupation of the two adjacent cavities in the above and below layers. The main result shows that in all cases but that of (1), Li generally prefers a location close to the centers of the four windows separating the A-type cage from the neighboring cavities within the same layer. This Li site is similar to that refined in the experimental neutron structures of tetragonal $Li_{0.3}La_{0.567}TiO_3$ (Li n.1, site S1). In case (1), Li goes to a different site vertically displaced from the center of the A-cavity, resembling site Li n.2, which was detected by Fourier maps but not refined in the experimental structures (site S2).

Therefore, it is now possible to associate the two disordered lithium sites found experimentally in the average tetragonal structure with the corresponding locally ordered configurations. Li takes the S1 or S2 site when its cavity lies in an "open" or "closed" environment, i.e., it is surrounded by few or by many La-occupied adjacent hollows. From the point of view of ionic mobility, the site S2 is clearly unfavorable, as the therein trapped Li ions have no surrounding sites available for jumping. Thus, processes of ion transfer should be based primarily on lithium hopping between sites n.1. These results are the starting step for kinetic modeling of ionic mobility in LLTO phases, which is now in progress.

Acknowledgment. A PRIN-COFIN financial support from MIUR (Rome) is gratefully acknowledged.

CM0709469